High-Order Switching Surface
in Boundary Control of Inverters

Julian Y.C. Chiu, Kelvin K.S. Leung, and Henry S.H. Chung*

Centre for Power Electronics
City University of Hong Kong
Kowloon Tong, Kowloon
Hong Kong
*Email: eeshc@cityu.edu.hk

Abstract - A high-order switching surface for boundary control of inverters is presented in this paper. The concept is based on using the natural response of the power stage to formulate a logarithmic function to approximate the ideal switching surface. With the proposed control method, the inverter exhibits better dynamic responses than the ones with the first-order or recently proposed second-order switching surfaces. It will also be shown that the first-order and second-order switching surfaces are the low-order approximations of high-order switching surface. As the high-order switching surface is close to the ideal switching surface, its high trajectory velocity along the switching surface makes the inverter state trajectory move toward the steady-state operating point in two switching actions under large-signal disturbances. The large-signal characteristics of the inverter will be discussed. The proposed control method has been successfully applied to a 300W, 110V, 60Hz, single-phase full-bridge inverter. The steady-state and large-signal dynamic behaviors of the inverter supplying to resistive, nonlinear inductive and full-wave rectifier loads will be given.

Index Terms – Boundary control, inverters, nonlinear control, inverter

I. INTRODUCTION

Apart from classical control theories [1]-[11], many recent works have focused on applying boundary-control-derived methods [12]-[23] to design controllers for switching inverters. Boundary control is a geometric based control approach suitable for switching converters [12, 13] featuring time-varying structures. Its advantage lies in its generality of controlling converter operation without differentiating startup, transient, and steady state periods, so it is possible to cope with large-signal disturbances in the input source and output load. The main objective of the boundary control method is to drive the converter to the steady state with the use of a switching surface to dictate the states of the switches. Typical switching surfaces used in switching converters are of first-order (σ^1), such as the sliding-mode control and hysteresis control [14]-[22].

Much research work extends the concept, such as using an adaptive approach in [24], in order to enhance the dynamics. Recently, the second-order switching surface (σ^2) has been proposed in [23]. It approximates the ideal switching surface ($\sigma*$) with a second-order function, in order to achieve the objective of settling switching transients in two switching actions. Since $\sigma*$ is load-dependent and σ^2 does not have the load information, the discrepancy between $\sigma*$ and σ^2 is dependent on the damping factor of the output circuit, or equivalently the value of the load impedance (Z) with respect to the output filter natural impedance (Z_C). Such discrepancy will increase if Z decreases and/or the converter state is far away from the operating point. Thus, this will make the

operating point during large-signal disturbances.

This paper gives a further enhancement on formulating the switching surface for inverters. A high-order switching surface (σ^N) is proposed. A logarithmic function is derived to approximate $\sigma*$. The inverter exhibits better dynamic response than the ones with σ^1 or σ^2. As the load characteristics is taken into account in the switching function, σ^N is close to $\sigma*$. The trajectory velocity along the switching surface is high that makes the trajectory ideally move toward the target operating point in two switching actions after a large-signal disturbance. The steady-state and large-signal characteristics have been studied. The proposed control method has been successfully applied to a 300W, 110V, 60Hz full-bridge inverter.
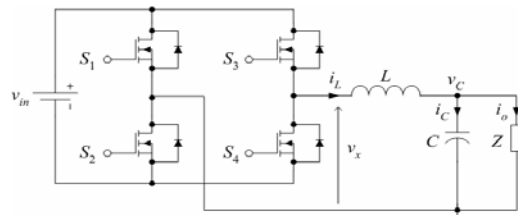
II. PRINCIPLES OF OPERATION

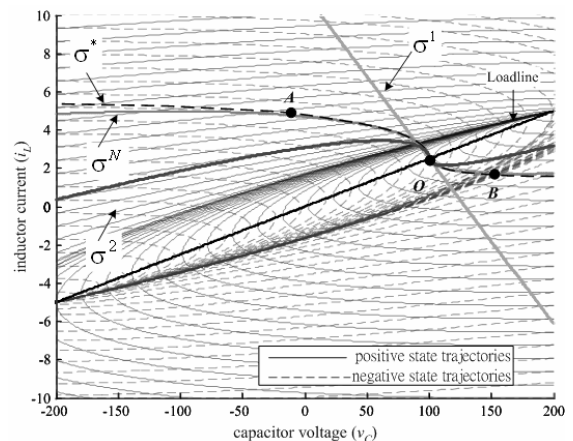Fig. 1 Schematic diagram of a full-bridge inverter.

Fig. 2 Families of trajectories.

TABLE I
COMPONENT USED IN THE SIMULATION AND PROTOTYPE

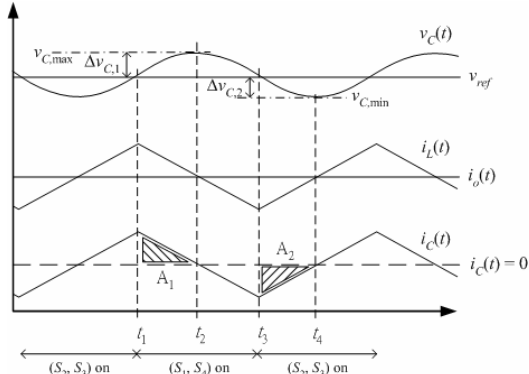| Parameter	Value
v_{in}	200 V
L	2mH
C	320nF

Fig. 3 Waveforms of v_C, i_L, i_o, and i_C.

Fig. 1 shows the schematic diagram of a full-bridge inverter, which can be described by the following state-space equations

$$\dot{x} = A_0 \, x + B_0 \, v_{in} + \left(A_1 \, x + B_1 \, v_{in} \right) q_1 + \left(A_2 \, x + B_2 \, v_{in} \right) q_2 \quad (1)$$

where $x = [\, i_L \quad v_C \,]$, i_L is the inductor current, v_C is the capacitor voltage and is equal to the load voltage, v_{in} is the input voltage, q_k represents the state of the switches, and A_k and B_k are constant matrices depending on the values of L, C, and the instantaneous ac load resistance R of the load Z. (S_2, S_3) are on if $\{q_1, q_2\} = \{1, 0\}$, and (S_1, S_4) are on if $\{q_1, q_2\} = \{0, 1\}$. Matrices A_0, B_0, A_1, B_1, A_2, and B_2 are defined as $A_0 = \begin{bmatrix} 0 & -1/L \\ 1/C & -1/RC \end{bmatrix}$, $B_0 = \begin{bmatrix} 0 \\ 0 \end{bmatrix}$,

$A_1 = \begin{bmatrix} 0 & 0 \\ 0 & 0 \end{bmatrix}$, $B_1 = \begin{bmatrix} 1/L \\ 0 \end{bmatrix}$, $A_2 = \begin{bmatrix} 0 & 0 \\ 0 & 0 \end{bmatrix}$, $B_2 = \begin{bmatrix} -1/L \\ 0 \end{bmatrix}$.

Fig. 2 shows families of trajectories that are obtained by solving (1) with different initial conditions. The inverter component values used are tabulated in Table I. The load is resistive and is given in Table II. The *positive state trajectories* are derived, when the inverter output voltage $v_x = v_{in}$ (i.e., with S_2 and S_3 on, and S_1 and S_4 off). The *negative state trajectories* are derived, when $v_x = -v_{in}$ (i.e., with S_2 and S_3 off, and S_1 and S_4 on). The tangential component of the trajectory velocity along the switching surface determines the rate at which successor points approach or recede from the operating point 'O' [12]. Depending on the location of the initial state, for example the states 'A' and 'B' in Fig. 2, the ideal switching surface (σ^*) is along either the only *positive state trajectory* or *negative state* trajectory that passes through 'O'. A switching surface that has deviation from σ^* will make the inverter require more switching actions to slide along the surface or to swirl around 'O' after a disturbance [12], [13] and [18] σ^2 has made a close approximation around the operating point. However, the settling time is still non-optimal under a large disturbance that significantly deviates from the operating point. A high-order switching surface (σ^N) that can well approximate σ^* is derived in this paper. With the help of the key waveforms shown in Fig. 3, the switching criteria are given as follows.

A. Criteria for switching on S_1 and S_4
As illustrated in Fig. 3, S_1 and S_4 are originally off and are switched on at the hypothesized time t_1. The objective is to determine t_1, so that $v_C(t_2) = v_{C,max}$ and $i_C(t_2) = 0$ after S_1 and S_4 are on, and the inverter will follow the negative state trajectory (Fig. 2). Thus, $v_C(t_1)$, $v_C(t_2)$, $i_C(t_1)$, and $i_C(t_2)$ are known values while t_2 is an unknown value. The following assumptions have been made in deriving the switching criteria,
1) The parasitic resistances of the switches, inductor, and capacitor are neglected.
2) For the sake of simplicity in the analysis and implementation, the values of v_C and the inductor voltage v_L in the considered interval $[t_1, \ t_2]$ are assumed to be constant. Their values are approximated by averaging their values at t_1 and t_2. They are denoted by $\overline{V}_{C,1}$ and $\overline{V}_{L,1}$, respectively. The approximation is applicable because the switching frequency is much higher than the frequency of the reference voltage v_{ref} and the variation of v_{ref} (and thus v_C and v_L) within a switching cycle is small. Thus,

$$v_C(t) = \overline{V}_{C,1} = \frac{v_C(t_1) + v_C(t_2)}{2}$$
$$= \frac{v_C(t_1) + v_{C,max}}{2} \quad (2)$$

$$v_L(t) = \overline{V}_{L,1} = -[v_{in} + \overline{V}_{C,1}]$$
and
$$= -\left[v_{in} + \frac{v_C(t_1) + v_{C,max}}{2} \right] \quad (3)$$

for $t_1 < t < t_2$.
By applying the Kirchoff's current law at the output node,

$$\frac{di_C(t)}{dt} + \frac{v_L(t)}{L} + \frac{i_C(t)}{CR} = 0 \quad (4)$$

where i_o is the output current and $R = \dfrac{\delta v_C}{\delta i_o}$ is the instantaneous ac load resistance.

By multiplying (4) with $e^{\frac{t}{CR}}$ and solving it for i_C, it can be shown that

$$i_C(t) = [i_C(t_1) - k_1] \, e^{\frac{t_1 - t}{CR}} + k_1 \quad (5)$$

where $k_1 = \dfrac{C \, R \, \overline{V}_{L,1}}{L}$.

Since $i_C(t_2) = 0$,

$$t_2 = C \, R \, \ln\left[1 - \frac{i_C(t_1)}{k_1} \right] + t_1 \quad (6)$$

and $\Delta v_{C,1} = v_C(t_2) - v_C(t_1) = v_{C,max} - v_C(t_1) = \dfrac{1}{C} \int_{t_1}^{t_2} i_C(t) \, dt$ (7)

By solving (7) with (5) and (6), the criteria for switching S_1 and S_4 on and S_2 and S_3 off are

$$v_C(t_1) \geq v_{C,max} - R \left[i_C(t_1) + k_1 \, \ln\left(1 - \frac{i_C(t_1)}{k_1} \right) \right]$$
and $\qquad\qquad i_C(t_1) > 0 \quad (8)$

B. Criteria for switching on S_2 and S_3
As illustrated in Fig. 3, S_2 and S_3 are originally off and are switched on at the hypothesized time t_3. The objective is to determine t_3, so that $v_C(t_4) = v_{C,min}$ and $i_C(t_4) = 0$

after S_2 and S_3 are on, and the inverter will follow the positive state trajectory (Fig. 2). Thus, $v_C(t_3)$, $v_C(t_4)$, $i_C(t_3)$, and $i_C(t_4)$ are known values while t_4 is an unknown value. Similar to Sec. A, the following assumptions have been made in deriving the switching criteria,

1) The parasitic resistances of the switches, inductor, and capacitor are neglected.

2) The values of v_C and the inductor voltage v_L in the considered interval $[t_3, t_4]$ are assumed to be constant. Their values are approximated by averaging their values at t_3 and t_4. They are denoted by $\overline{V}_{C,2}$ and $\overline{V}_{L,2}$, respectively. That is,

$$v_C(t) = \overline{V}_{C,2} = \frac{v_C(t_3) + v_C(t_4)}{2}$$
$$= \frac{v_C(t_3) + v_{C,\min}}{2} \tag{9}$$

$$v_L(t) = \overline{V}_{L,2} = v_{in} - \overline{V}_{C,2}$$

and
$$= v_{in} - \frac{v_C(t_3) + v_{C,\min}}{2} \tag{10}$$

for $t_3 < t < t_4$.

Again, by using (4) and similar technique for calculating (5), it can be shown that

$$i_C(t) = [i_C(t_3) - k_2] e^{\frac{t_3 - t}{CR}} + k_2 \tag{11}$$

where $k_2 = \dfrac{C R \overline{V}_{L,2}}{L}$.

Since $i_C(t_4) = 0$,

$$t_4 = C R \ln\left[1 - \frac{i_C(t_3)}{k_2}\right] + t_3 \tag{12}$$

and $\Delta v_{C,2} = v_C(t_4) - v_C(t_3) = v_{C,\min} - v_C(t_3) = \dfrac{1}{C} \int_{t_3}^{t_4} i_C(t)\, dt$ (13)

By solving (13) with (11) and (12), the criteria for switching S_2 and S_3 on, and S_1 and S_4 off are

$$v_C(t_3) \le v_{C,\min} - R\left[i_C(t_3) + k_2 \ln\left(1 - \frac{i_C(t_3)}{k_2}\right)\right]$$

and
$$i_C(t_3) < 0 \tag{14}$$

Fig. 3 shows the waveforms of the inverter with hysteresis bands added, in order to avoid frequency chattering. However, for the sake of simplicity in design and analysis, the hysteresis band is ignored in the calculations. Thus, by combining (8) and (14) and putting $v_{C,\min} = v_{C,\max} = v_{ref}$, the following switching surface σ^N is defined

$$\sigma^N(i_L, v_C) = \begin{cases} R\left[i_C + k_1 \ln\left(1 - \frac{i_C}{k_1}\right)\right] + (v_C - v_{ref}) \\[2ex] R\left[i_C + k_2 \ln\left(1 - \frac{i_C}{k_2}\right)\right] + (v_C - v_{ref}) \end{cases} \tag{15}$$

where $i_C = i_L - \dfrac{v_C}{R}$.

The equation can be written into a general form of

$$\sigma^N(i_L, v_C) = R\left[i_C + c_1 \ln\left(1 - \frac{i_C}{c_1}\right)\right] + (v_C - v_{ref}) \tag{16}$$

where $c_1 = \dfrac{k_1}{2}[1 + \mathrm{sgn}(i_C)] + \dfrac{k_2}{2}[1 - \mathrm{sgn}(i_C)]$ and $i_C = $

$i_L - \dfrac{v_C}{R}$.

Fig. 2 shows σ^N in the state plane. Fig. 4 shows the block diagram of the proposed high-order boundary controller.
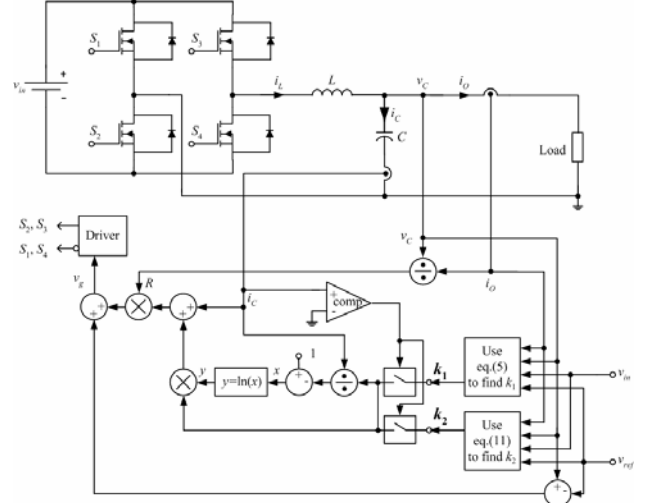

Fig. 4 Block diagram of the proposed high-order boundary controller.

III. Comparisons among σ^*, σ^1, σ^2, and σ^N

By expanding the logarithmic function in (16) with the Taylor series,

$$\sigma^N\big|_{N\to\infty} = R\left[i_C + c_1\left[\sum_{n=1}^{N} -\frac{1}{n}\left(\frac{i_C}{c_1}\right)^n\right]\right] + (v_C - v_{ref}) \tag{17}$$

and putting $N = 0, 1, 2$ respectively, it can be shown that

$$\sigma^N\big|_{N=0} = R\, i_C + (v_C - v_{ref}) \tag{18}$$

$$\sigma^N\big|_{N=1} = v_C - v_{ref} \tag{19}$$

$$\sigma^N\big|_{N=2} = -\frac{R}{2}\frac{i_C^2}{c_1} + (v_C - v_{ref}) \tag{20}$$

Eq. (18) gives the typical mathematical expression of the switching surface for the sliding-mode control. Eq. (19) gives the typical expression switching surface for the hysteresis control. By substituting the values of k_1 in (5) and k_2 in (11) for c_1 in (20), it can be shown that

$$\sigma^N\big|_{N=2} = \frac{L\, i_C^2}{2 C \left(v_{in} + \frac{v_C + v_{ref}}{2}\right)} + (v_C - v_{ref}) \tag{21}$$

for switching S_1 and S_4 on and S_2 and S_3 off, and

$$\sigma^N\big|_{N=2} = -\frac{L\, i_C^2}{2 C \left(v_{in} - \frac{v_C + v_{ref}}{2}\right)} + (v_C - v_{ref}) \tag{22}$$

for switching S_2 and S_3 on and S_1 and S_4 off.

Eqs. (21) and (22) give similar expressions as the switching surface σ^2 proposed in [23]. Thus, σ^2 is also the low-order approximation of σ^N.

In the following analysis, a pure mathematical treatment on comparing the discrepancies of σ^1, σ^2, and σ^N with σ^* is conducted. All switching surfaces are considered as continuous mathematical functions. No intracycle switching behaviors are taken into account. For the sake of comparison the values of v_c and i_c along the respective switching surface are normalized by the values at the operating point. The switching surfaces are compared by studying those surfaces on a $\hat{i}_c$-$\hat{v}_c$ plane, where $\hat{i}_c$

and $\hat{v}_C$ are the normalized values of i_C and v_C, respectively.

v_C is normalized by the base value of v_{ref}. That is,

$$\hat{v}_C = \frac{v_C}{v_{ref}} \qquad (23)$$

i_C is normalized by the base value of $i_{C,n}$, which is equal to

$$i_{C,n} = \frac{v_{ref}}{Z_C} \qquad (24)$$

where $Z_C = \frac{1}{2}\sqrt{\frac{L}{C}}$ is the load impedance that the output filter is in critical damping.

Thus,

$$\hat{i}_C = \frac{i_C}{i_{C,n}} \qquad (25)$$

By putting (23) and (25) into (16), (18), and (20), the normalized switching surfaces $\hat{\sigma}^N$, $\hat{\sigma}^1$, and $\hat{\sigma}^2$ of σ^N, σ^1, and σ^2, respectively, with different load resistances are equal to

$$\hat{\sigma}^1 = R\hat{i}_C + Z_C\hat{v}_C - Z_C \qquad (26)$$

$$\hat{\sigma}^2 = c_1\hat{i}_C^{\,2} + \frac{Z_C^{\,2}}{v_{ref}}\hat{v}_C - \frac{Z_C^{\,2}}{v_{ref}} \qquad (27)$$

$$\hat{\sigma}^N = R\left[\hat{i}_C + c_1\frac{Z_C}{v_{ref}}\ln\left(1 - \frac{v_{ref}}{Z_C}\frac{\hat{i}_C}{c_1}\right)\right] + (Z_C\hat{v}_C - Z_C) \quad (28)$$

When the inverter reaches the steady state, $v_C = v_{ref}$ and $i_C = 0$. Thus, the normalized operating point ($\hat{v}_{C,o}$, $\hat{i}_{C,o}$) on the $\hat{i}_C$-$\hat{v}_C$ plane is

$$\hat{v}_C = 1 \qquad (29)$$

and

$$\hat{i}_C = 0 \qquad (30)$$

The normalized ideal switching surface $\hat{\sigma}^*$ is obtained by putting (23) and (25) into (1). A comparison of $\hat{\sigma}^1$, $\hat{\sigma}^2$, $\hat{\sigma}^N$, and $\hat{\sigma}^*$ is shown in Fig. 5. Among them, $\hat{\sigma}^1$ deviates considerably from $\hat{\sigma}*$, $\hat{\sigma}^2$ gives closer approximation to $\hat{\sigma}*$ around the operating point, and $\hat{\sigma}^N$ gives the best approximation of $\hat{\sigma}*$ over the operating range.

Figs. 6 shows the comparisons of the simulated time-domain waveforms, including v_C, i_L, and the gate signal to S_2 and S_3, v_g, and the state-space trajectories with various switching surfaces under a large-signal reference voltage change from the peak voltage of $70V_{rms}$ (i.e., 99V) to $110V_{rms}$ (i.e., 155V) and vice versa. The parameters used are given in Table I. The settling times of the system with different switching surfaces are given in Table III. It can be observed that the one with σ^N gives the shortest settling time, confirming the advantages of the proposed control.
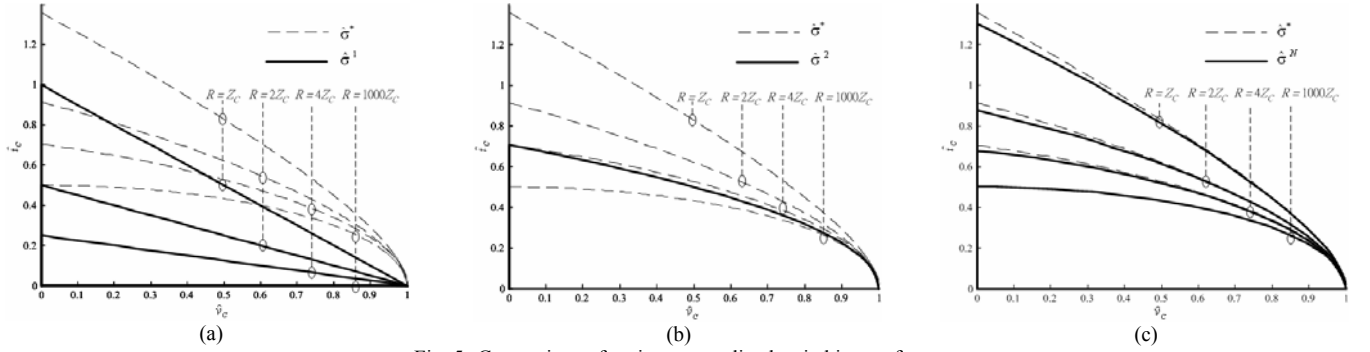

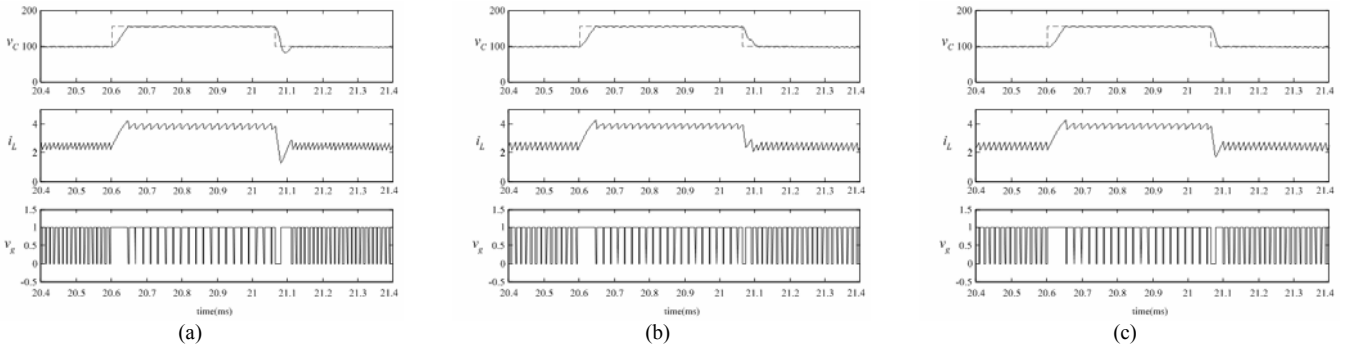Fig. 5 Comparison of various normalized switching surfaces.

Fig. 6 Simulated time-domain waveforms of the inverter various switching surfaces under large-signal reference changes. (a) σ^1. (b) σ^2. (c) σ^N.

VI. LARGE-SIGNAL CHARACTERISTICS

Points along $\sigma^N = 0$ in (16) can be classified into refractive, reflective, and rejective modes. The dynamics of the system behaves differently in those regions [18] and is studied by observing the correlation between the transition boundary and the switching surface. Basically,

the value of c_1 in (16) determines the dynamic characteristics. Assume that c_1 is a factor of the ideal value of k_1, as defined in (5), when S_1 and S_4 are on. That is,

$$c_1 = \zeta_{S_{1,4}}k_1 \qquad (31)$$

where $\zeta_{S_{1,4}}$ is the discrepancy factor. If $\zeta_{S_{1,4}} = 1$, the inverter follows the derived switching surface. As there

are discrepancies between the ideal component values and the actual component values, $\zeta_{S_{1,4}} \neq 1$, resulting in behaving non-ideal dynamic response.

The transition boundary with S_1 and S_4 on is obtained by differentiating (16) and substituting $\left. \dfrac{d\,i_L}{d\,v_C} \right|_{S_{1,4}}$ which obtained by using (1). Thus,

$$
\begin{aligned}
R &\left[i_L - \frac{v_C}{R} - \left(\frac{CR}{L}\frac{v_{in}+v_C}{v_{in}+v_{ref}}(v_{in}+\frac{v_C+v_{ref}}{2}) + \frac{R}{2}\frac{(i_L-\frac{v_C}{R})(i_L-\frac{v_{ref}}{R})}{(v_{in}+v_{ref})} \right) \right. \\
&\left. \cdot \ln\left| 1 + \frac{i_L - \frac{v_C}{R}}{\frac{CR}{L}\frac{v_{in}+v_C}{v_{in}+v_{ref}}(v_{in}+\frac{v_C+v_{ref}}{2}) + \frac{R}{2}\frac{(i_L-\frac{v_C}{R})(i_L-\frac{v_{ref}}{R})}{(v_{in}+v_{ref})}} \right| \right] \\
&+ (v_C - v_{ref}) = 0
\end{aligned}
\tag{32}
$$

Similarly, the transition boundary with S_2 and S_3 on is obtained by differentiating (16) that

$$c_1 = \zeta_{S_{2,3}}\,k_2 \tag{33}$$

where $\zeta_{S_{2,3}}$ is the discrepancy factor between c_1 and the ideal value of k_2, as defined in (11). If $\zeta_{S_{2,3}} = 1$, the inverter follows the derived switching surface. By using (1), $\left. \dfrac{d\,i_L}{d\,v_C} \right|_{S_{2,3}}$ can also be obtained. Thus,

$$
\begin{aligned}
R &\left[i_L - \frac{v_C}{R} + \left(\frac{CR}{L}\frac{v_{in}-v_C}{v_{in}-v_{ref}}(v_{in}-\frac{v_C+v_{ref}}{2}) + \frac{R}{2}\frac{(i_L-\frac{v_C}{R})(i_L-\frac{v_{ref}}{R})}{(v_{in}-v_{ref})} \right) \right. \\
&\left. \cdot \ln\left| 1 - \frac{i_L - \frac{v_C}{R}}{\frac{CR}{L}\frac{v_{in}-v_C}{v_{in}-v_{ref}}(v_{in}-\frac{v_C+v_{ref}}{2}) + \frac{R}{2}\frac{(i_L-\frac{v_C}{R})(i_L-\frac{v_{ref}}{R})}{(v_{in}-v_{ref})}} \right| \right] \\
&+ (v_C - v_{ref}) = 0
\end{aligned}
\tag{34}
$$

As shown in Fig. 7(a), if the values of $\zeta_{S_{1,4}} = \zeta_{S_{2,3}} = 1$, the switching surface lies along the transition boundaries and is between the reflective and refractive regions when it is close to the operating point. This leads to good dynamic response to disturbances that the converter will settle to the steady state in two switching actions. However, the switching surface starts deviating from the transition boundaries, when the state point is far from the operating point. This is consistent with the comparison of σ^* and σ^N shown in Fig. 5. The inverter will then require more switching cycles to settle under a large-signal disturbance.

Fig. 7(b) shows the transition boundaries and the switching surface with $\zeta_{S_{1,4}} = \zeta_{S_{2,3}} = 0.5$. The switching surface almost lies on the reflective region. The implication is that the inverter is operating in sliding mode when it is subject to external disturbance.

Fig. 7(c) shows the transition boundaries and the switching surface with $\zeta_{S_{1,4}} = \zeta_{S_{2,3}} = 2$. The whole switching surface almost lies on the refractive region. The implication is that the inverter's trajectory will move toward the operating point in a spiral manner.

With $\zeta_{S_{1,4}}$ and/or $\zeta_{S_{2,3}}$ not equal to unity, the inverter will requires more switching actions before getting into the steady-state operating point.

VII. EXPERIMENTAL VERIFICATIONS

A 300W, 110V, 60Hz full bridge inverter has been built and tested. The component values are tabulated in Table I.

Fig. 8 shows the enlarged waveforms of the dynamic responses of the inverter supplying to the 40Ω resistive load with different switching surfaces, including σ^N, σ^2 and σ^1. The reference voltage is suddenly changed at the peak of the reference signal from 70V$_{rms}$ to 110V$_{rms}$. Among them, σ^N gives the best dynamic response. As shown in Fig. 8(c), the inverter only takes two switching actions getting into the steady state.

Fig. 9 shows the steady-state output voltage waveforms supplying to resistive, nonlinear inductive, and full-wave rectifier loads. The output voltage is sinusoidal in all cases. The load specifications are tabulated in Table II.

Fig. 10 shows the harmonic spectra of the output voltage with different loads. The third harmonics (180Hz) is less than the fundamental component (60Hz) by more than 45dB in both cases. The THD of the output voltage is less than 1.1%. Fig. 11 shows the transient responses of the output voltage when the resistive load is changed from the rated load to 20% load, and vice versa. The inverter can revert to the steady state in two to three switching actions.

TABLE II
LOAD SPECIFICATION OF THE PROTOTYPE

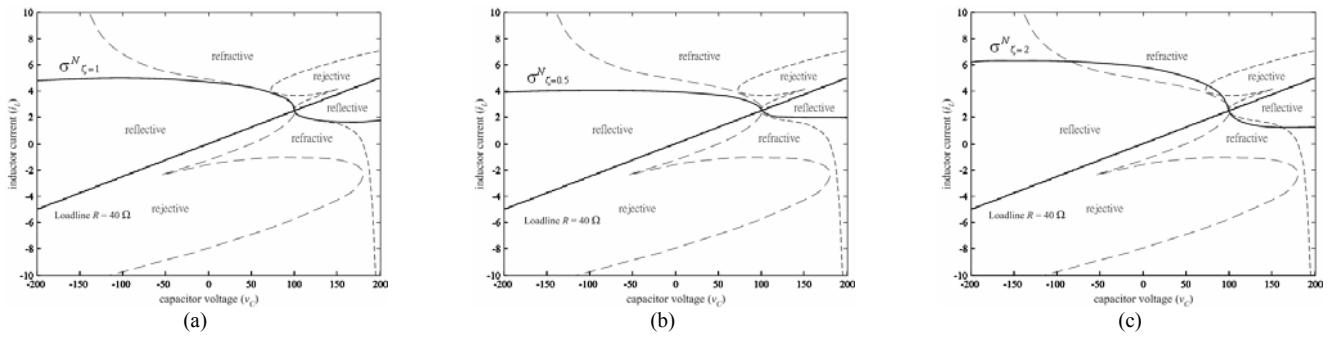| Load (Z)	Value
Resistive	40Ω
Nonlinear Inductive	23mH + 40Ω
Full-wave rectifier load	264μF + 240Ω

Fig. 7 Illustration of the switching surfaces and switching boundaries. (a) k_1 and k_2 are ideal ($\zeta_{S_{1,4}} = \zeta_{S_{2,3}} = 1$). (b) k_1 and k_2 are one half of the ideal values ($\zeta_{S_{1,4}} = \zeta_{S_{2,3}} = 0.5$). (c) k_1 and k_2 are twice the ideal values ($\zeta_{S_{1,4}} = \zeta_{S_{2,3}} = 2$).
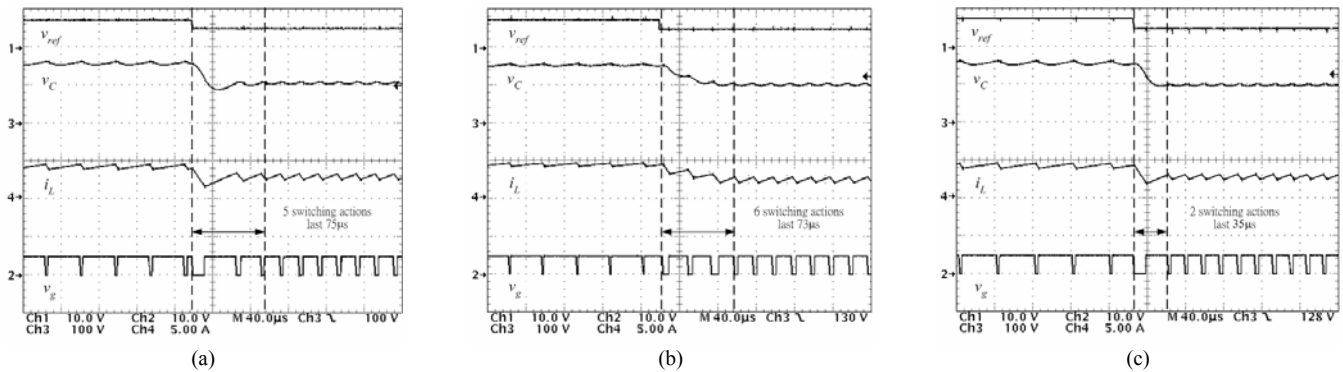

Fig. 8 Dynamic response of the inverter when the reference signal is changed from 110 V$_{rms}$ to 70 V$_{rms}$ at the angle around 90° [Ch1: v_{ref} (10 V/div), Ch2: v_g (10 V/div), Ch3: v_C (100 V/div), Ch4: i_L (5 A/div), timebase: 40μs/div].
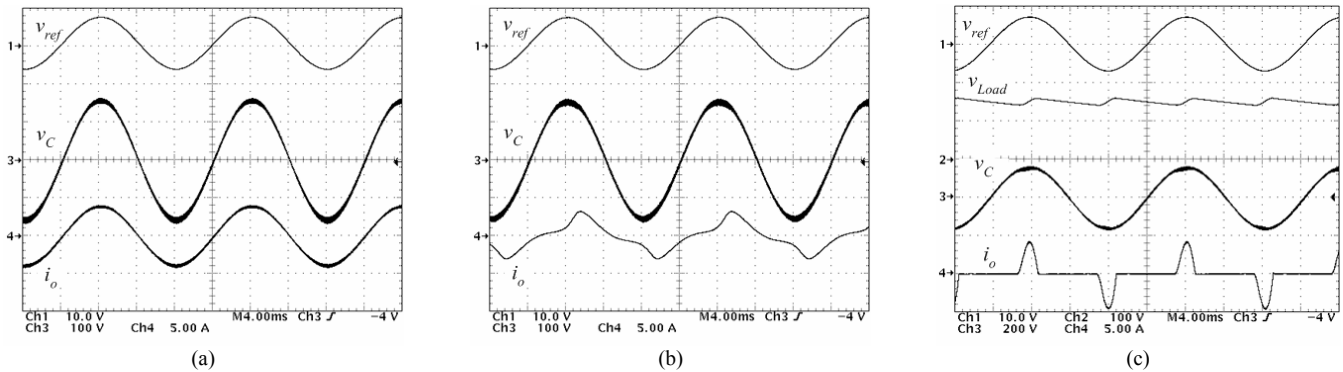

Fig. 9 Steady-state operations of the inverter [Ch1: v_{ref} (10 V/div), Ch2: v_{Load} (100V/div), Ch3: v_C (100 V/div), Ch4: i_o (5 A/div), timebase: 4ms/div]. (a) Resistive load. (b) Nonlinear inductive load. (c) Full-wave rectifier load.
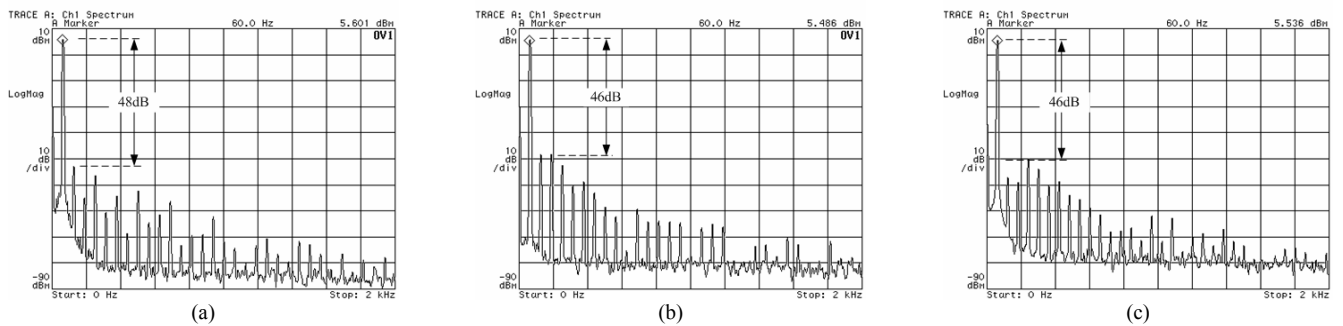

Fig. 10 Harmonic spectra of the output voltage. (a) Resistive load. (b) Nonlinear inductive load. (c) Full-wave rectifier load.

<div style="text-align:center">(a)   (b)</div>

Fig. 11   Transient responses under load changes.   (a) Rated load to 20% load.   (b) 20% load to rated load.   [Ch1: i_o (2 A/div), Ch2: v_g (10 V/div), Ch3: v_C (100 V/div), Ch4: i_L (5 A/div) , timebase: 40μs/div].

VIII. Conclusions

To conclude this paper,

- A high-order switching surface for boundary control of inverters has been presented.   An generalized equation has been derived in (16).
- It has also been shown that the first- and second-order switching surfaces are the low-order approximation of σ^N in (26)-(28)
- The control method has been applied to DC-AC inverter successfully and does not require any sophisticated calculations of the transfer functions or closed-loop compensation.   The controller's parameters are obtained readily by considering the component values of the power stage.   It is unnecessary to determine the controller parameters by the trail-and-error approach.
- The proposed method has applied to the inverter with different load types and performs well in large-signal variations.
- The proposed method has been confirmed experimentally.
- Further research will be dedicated into the boundary control with constant switching frequency.

References

[1]   K. Taniguchi, Y. Ogino, and H. Irie, "PWM Technique for Power MOSFET Inverter," *IEEE Trans. on Power Electronics*, vol. 3, no. 3, pp. 328-334, July 1988.

[2]   J. Holtz, "Pulsewidth Modulation for Electronic Power Conversion," *Proc. IEEE*, vol. 82, pp.1194-1214, Aug. 1994.

[3]   J. W. Kolar, H. Ertl, and F. C. Zach, "Influence of the Modulation Method on the Conduction and Switching Losses of a PWM Converter System," *IEEE Trans. on Industry Applications*, vol. 27, no. 6, pp. 1063-1075, Nov.-Dec. 1991.

[4]   H. Kim, H. Lee and S. Sul, "A new PWM strategy for common-mode voltage reduction in neutral-point-clamped inverter-fed AC motor drives," *IEEE Trans. On Industry App.*, vol. 37, no. 6, pp. 1840-1845, Nov/Dec 2001.

[5]   M. Kojima, K. Hirabayashi, Y. Kawabata, E. C. Ejiogu and T. Kawabata, "Novel Vector Control System Using Deadbeat-Controlled PWM Inverter with Output LC Filter," *IEEE Trans. on Industry App.*, vol. 40, no. 1, pp. 162-169, Jan-Feb 2004.

[6]   K. Zhang, Y. Kang, J. Xiong and J. Chen, "Direct Repetitive Control of SPWM Inverter for UPS Purpose," *IEEE Trans. on Power Electronics*, vol. 18, no. 3, pp. 784-792, May 2003.

[7]   O. Kukrer, H. Komurcugil and N. S. Bayindir, " Control Strategy for Single-Phase UPS inverter," in *Proc. IEE Electric Power App.*, vol. 150, no. 6, pp. 743-746, Nov. 2003.

[8]   S. R. Bowes, D. Holliday and S. Grewal, "Regular-Sampled Harmonic Elimination PWM Control of Single-Phase Two-Level Inverters," in *Proc. IEE Electric Power App.*, vol. 148, no. 4, pp. 309-314, Jul. 2001.

[9]   N. Hur, J. Jung, and K. Nam, "A Fast Dynamic DC-Link Power-Balancing Scheme for a PWM Converter-Inverter System," *IEEE Trans. on Industrial Electronics*, vol. 48, no. 4, pp. 794-803, August 2001.

[10]   J. C. Liao and S. N. Yeh, "A Novel Instantaneous Power Control Strategy and Analytic Model for Integrated Rectifier / Inverter Systems," *IEEE Trans. on Power Electronics*, vol. 15, no. 6, pp. 996-1006, Nov. 2000.

[11]   J. Holtz and B. Beyer, "Optimal Synchronous Pulsewidth Modulation with a Trajectory-Tracking Scheme for High-Dynamic Performance," *IEEE Trans. on Industry Applications*, vol. 29, no. 6, pp. 1098-1105, Nov.-Dec. 1993.

[12]   R. Munzert and P. T. Krein, "Issues in boundary control," in *Proc., IEEE Power Electron. Spec. Conf.,* 1996, pp. 810-816.

[13]   R. M. Bass and P. T. Krein, "Switching boundary geometry and the control of single-phase inverters," in *Proc., IEEE Industry Applications Society Annual Meeting,* 1989, pp. 1052-1056.

[14]   S. H. Jung, N. I. Kim, and G. H. Cho, "Class D audio power amplifier with fine hysteresis control," *IEEE Electronics Letters*, vol. 38, no.2, pp. 1302-1303, Oct. 2002.

[15]   T. L. Tai, and J. S. Chen, "UPS Inverter Design Using Discrete-Time Sliding-Mode Control Scheme," *IEEE Trans. on Industrial Electronics*, vol.49, no. 1, pp. 67-75, Feb. 2002.

[16]   H. Ma and S. Han, "Analysis and Design of Sliding Mode Control for AC Signal Power Amplifier," *IEEE Industrial Electron. Soc. Conf.*, vol. 2, pp. 1652-1657, Nov. 2004.

[17]   E. Chang, T. Lian, J. Chen, and R. Lin, "A Sliding-Mode Controller based on Fuzzy Logic for PWM Inverters," in *Proc. IEEE Asia-Pacific Conf. on Circuit and Systems*, vol. 2, pp. 965-968, Dec. 2004.

[18]   M. Greuel, R. Muyshondt, and P. T. Krein, "Design Approaches to Boundary Controllers" in *Proc., IEEE Power Electron. Spec. Conf.*, 1997, pp. 672-678.

[19]   D. Biel, E. Fossas, F. Guinjoan, E. Alarcon, and A. Poveda, "Application of Sliding-Mode Control to the Design of a Buck-Based Sinusoidal Generator," *IEEE Trans. on Power Electronics*, vol. 48, no. 3, pp. 563-571, June 2001.

[20]   R. R. Ramos, D. Biel, E. Fossas, and F. Guinjoan, "A Fixed-Frequency Quasi-Sliding Control Algorithm: Application to Power Inverters Design by Means of FPGA Implementation," *IEEE Trans. on Power Electronics*, vol. 18, no. 1, pp. 344-355, January 2003.

[21]   W. M. P. Filho and A. J. Perin, "An Approach of the Variable Structure Analysis for Power Electronics Applications," in *Proc., IEEE Industry Applications Society Annual Meeting,* 1997, pp. 844-851

[22]   S. C. Tan, Y. M. Lai, C. K. Tse and M. K. H. Cheung, "Adaptive Feedforward and Feedback Control Schemes for Sliding Mode Controlled Power Converters," *IEEE Trans. on Power Electronics*, vol. 21, no. 1, pp. 182-192, Jan. 2006.

[23]   K. K. S. Leung and H. S. H. Chung, "Derivation of a Second-Order Switching Surface in the Boundary Control of Buck Converters," *IEEE Power Electronics Letter*, vol. 2, no. 2, pp. 63-67, June 2004.

[24]   V. M. Nguyen and C. Q. Lee, "Tracking control of buck converter using sliding-mode with adaptive hysteresis," in *Proc., IEEE Power Electron. Spec. Conf.*, 1995, pp. 1086-1093.